

Superconductivity in the cobalt-doped V₃Si A15 intermetallic compound

Lingyong Zeng^{a, #}, Huawei Zhou^{a, #}, Hong Du^b, Ruidan Zhong^b, Ruixin Guo^{c, d}, Shu Guo^{c, d}, Wanzhen Su^a, Kuan Li^a, Chao Zhang^a, Peifeng Yu^a, Huixia Luo^{a}*

^aSchool of Materials Science and Engineering, State Key Laboratory of Optoelectronic Materials and Technologies, Key Lab of Polymer Composite & Functional Materials, Guangzhou Key Laboratory of Flexible Electronic Materials and Wearable Devices, Sun Yat-Sen University, No. 135, Xingang Xi Road, Guangzhou, 510275, P. R. China.

^bTsung-Dao Lee institute , Shanghai Jiao Tong University, Shanghai, 200240, P. R. China.

^cShenzhen Institute for Quantum Science and Engineering, Southern University of Science and Technology, Shenzhen 518055, China.

^dInternational Quantum Academy, Shenzhen 518048, China.

[#] These authors contributed equally to this work.

^{*}Corresponding author' email address: luohx7@mail.sysu.edu.cn; complete details (Telephone and Fax) (+0086)-2039386124

Abstract

The A15 structure of superconductors is a prototypical type-II superconductor that has generated considerable interest since the early history of superconducting materials. This paper discusses the superconducting properties of previously unreported $V_{3-x}Co_xSi$ ($0 \leq x \leq 0.30$) alloys. It is found that the lattice parameter decreases with increasing cobalt-doped content and leads to an increased residual resistivity ratio (RRR) value of the $V_{3-x}Co_xSi$ system. Meanwhile, the superconducting transition temperature (T_c) decreases with increasing cobalt-doped content. Furthermore, the fitted data show that the increase of cobalt-doped content also reduces the lower/upper critical fields of the $V_{3-x}Co_xSi$ system. Type-II superconductivity is demonstrated on all $V_{3-x}Co_xSi$ samples. With higher Co-doped content, $V_{3-x}Co_xSi$ ($0.15 \leq x \leq 0.30$) alloys may have superconducting and structural phase transitions at low-temperature regions. As the electron/atom (e/a) ratio increases, the T_c variation trend of V_3Si is as pronounced as in crystalline alloys and monotonically follows the trend observed for amorphous superconductors.

Keywords: A15 structure; superconductivity; $V_{3-x}Co_xSi$; electron/atom ratio

Introduction

Superconductors with the cubic A15 structure, discovered mainly between the 1950s and 1970s, represent metal-based superconductors [1-5]. Until the copper-oxide superconductors were discovered in 1986, the A15 structure held the record highest superconducting transition temperature (T_c), around 23 K for Nb₃Ge [6,7], which has since been commercialized. A15 intermetallic compounds with the general formula A₃B are one of the most extensively studied materials owing to their relatively high T_c values and rich physical properties. Recently, the first-principles calculations indicate that the bulk electronic band structures of Ta₃Sb, Ta₃Sn, and Ta₃Pb have nontrivial band topologies, inducing the formation of topological surface states near the Fermi energy [8]. The A15 superconductors are promising candidates for the realization of topological superconductivity and the Majorana fermion.

V₃Si is a well-known A15-type superconductor with the T_c around 17 K and 4.7 electrons per atom (e/a) [9]. Despite its simple cubic structure at room temperature, most transport, thermodynamic and spectroscopic measurements exhibited unconventional behavior or at least some unusual features [10-15]. Such as anisotropy of the upper critical field and specific heat, de Hass-van Alphen effect, and large ratio of T_c with Fermi temperature (T_F). Strong evidence exists that a martensitic cubic to tetragonal phase transition occurs at about 18.9 K, slightly above the T_c [16-19]. Unusual softening of the acoustic phonons in V₃Si has been reported [20,21]. And the inelastic x-ray scattering investigation of the lattice dynamics of V₃Si indicates only a small impact of the soft phonon mode of the martensitic transition on the superconducting properties [17]. The theoretical analysis and experimental results recently present strong support for an s⁺⁺ pairing with two barely coupled gaps and weak interband coupling in the V₃Si superconductor [22], which is very similar to the MgB₂ superconductor [23]. Besides, V₃Si thin films can reach T_c up to 15 K, depending on the substrate properties and the annealing temperature [24,25]. Due to the above physical properties, V₃Si is still a good material platform to study physical properties, especially superconductivity. A flexible and effective method for illuminating the fundamental properties of superconductivity is the modulation of T_c through carrier

concentration. [26,27]. To improve V_3Si 's superconducting properties, many chemical doping studies have been conducted. [28-30]. Nevertheless, it is still a lack of study on doping cobalt into V_3Si . In addition, cobalt has been widely used as a dopant to regulate the superconducting parameters or magnetic properties in iron-based superconductors (e.g., $LaFe_{1-x}Co_xAsO$, $SmFe_{1-x}Co_xAsO$, $CeFe_{1-x}Co_xAsO$, and $Fe_{1-x}Co_xO$) and cuprate superconductors ($YBa_2Cu_{3-x}Co_xO_{7\pm\delta}$) [31-34]. Furthermore, it is still necessary to systematically study the correlation between the valence electron count (VEC) and T_c in the V_3Si system, especially in the region $e/a > 4.7$. The cobalt element ($3d^74s^2$) has 9 electrons, which is more than the 5 electrons of the vanadium element ($3d^34s^2$). The cobalt doping thus will increase the number of e/a in the V_3Si ($e/a = 4.7$) system.

In this work, magnetic cobalt ($3d^74s^2$) dopants on the vanadium site of V_3Si were prepared, and superconducting properties of $V_{3-x}Co_xSi$ ($0 \leq x \leq 0.30$) were systemically studied. Experimental data indicate that cobalt doping gradually suppresses T_c , accompanied by an increment of the e/a ratio. The fitted data show that the increase of cobalt-doped content also reduces the critical field of the $V_{3-x}Co_xSi$ system. Type-II superconductivity is demonstrated on $V_{2.975}Co_{0.025}Si$ alloy, whose lower critical field ($\mu_0H_{c1}(0)$) is 1.2 T and upper critical field ($\mu_0H_{c2}(0)$) is 30.0 T. With higher Co-doped content, $V_{3-x}Co_xSi$ ($0.15 \leq x \leq 0.30$) alloys may have superconducting and structural phase transitions.

Experimental

The polycrystalline samples $V_{3-x}Co_xSi$ ($0 \leq x \leq 0.30$) were synthesized through an arc-melting method. Stoichiometric mixtures of V (99.5%, Aladdin), Co (99.5%, Alfa Aesar), and Si (99.99%, Macklin) powders were well-ground together, pressed into a cylinder and placed into a water-cooled melting furnace. They were arc melted in an argon atmosphere and rapidly cooled. The samples were subsequently annealed at 1000 °C under a vacuum. The weight loss during the melting process is almost negligible.

Powder x-ray diffraction (PXRD) collected the phase composition and lattice structure information from powdered samples at room temperature. We analyze the PXRD data with the Rietveld refinement model of the Fullprof suite software.

Microstructural characterization of the samples was conducted by scanning electron microscope (SEM, EVO MA10) with energy dispersive spectroscopy (EDS). Temperature-dependent resistivity (four-point probe), zero-field-cooling (ZFC) magnetic susceptibility, and heat capacity were determined through the physical property measurement system (PPMS, DynaCool, Quantum Design, Inc).

Results and discussion

PXRD has been recorded for identifying the composition and crystal structure of $V_{3-x}Co_xSi$ ($0 \leq x \leq 0.30$) alloys. **Fig. 1(a)** presents the detailed refinement of the typical compound $V_{2.92}Co_{0.08}Si$ at room temperature. All the diffraction peaks are crystallized in the cubic structure with $Pm-3n$ space group. A good agreement is obtained between calculated and observed patterns, which is corroborated by the small χ^2 (2.4214) factor. The inset in **Fig. 1(a)** displays the $V_{3-x}Co_xSi$ crystal structure based on the refinement results. The cobalt concentration is limited up to 0.3 since CoSi impurity becomes apparent as cobalt concentration is increased. As the cobalt-doped concentration increases, the (210) peak shifts to a lower Bragg angle, which is evident from the decrease in lattice constant a with increasing x , implying the compression of the V_3Si unit cell. Tiny V impurities are discovered in some cobalt-doped samples (see **Fig. 1(b)**). The relevant refined lattice parameters for $V_{3-x}Co_xSi$ ($0 \leq x \leq 0.30$) examples are shown in **Fig. 1(c)**. The lattice parameters monotonically decrease trend with enhancing cobalt-doped content, which can be attributed to the slightly smaller atomic radius of cobalt (125 pm) than vanadium (134 pm). It shows that the lattice constant a reduces from 4.7243(1) Å of the pristine sample V_3Si to 4.7061(2) Å of the highest doping $V_{2.7}Co_{0.3}Si$ compound. The SEM-EDS was performed to confirm the elements' distribution and the accurate ratio in the $V_{3-x}Co_xSi$ system. As shown in **Fig. 2**, a homogeneous elemental distribution was observed in the $V_{3-x}Co_xSi$ system. The cobalt is indeed in our doping alloys, and the actual cobalt ratios are very close to the designed ratios (see **Table 1**).

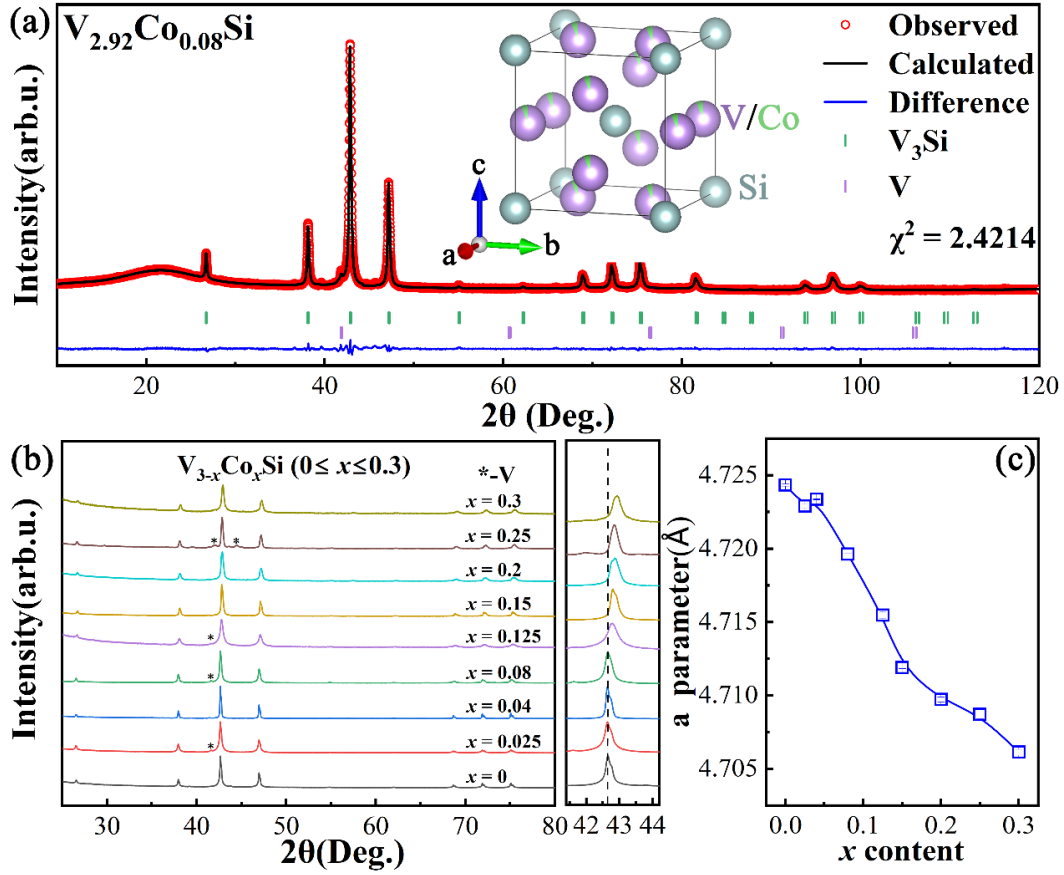


Fig. 1 (a) PXRD refinement of $V_{2.92}Co_{0.08}Si$. The inset shows the crystal structure of $V_{3-x}Co_xSi$ alloys with space group $Pm-3n$. (b) PXRD pattern of $V_{3-x}Co_xSi$ alloys. (c) Cobalt-doped content dependence of the lattice parameter a of $V_{3-x}Co_xSi$ alloys.

Table 1. The element ratios of $V_{3-x}Co_xSi$ from EDS results.

Element ratio	V	Si	Co
Sample			
V_3Si	3.2	0.8	0
$V_{2.975}Co_{0.025}Si$	3.13	0.85	0.02
$V_{2.96}Co_{0.04}Si$	3.16	0.8	0.04
$V_{2.92}Co_{0.08}Si$	3.07	0.85	0.08
$V_{2.85}Co_{0.15}Si$	3	0.85	0.15
$V_{2.8}Co_{0.2}Si$	3.01	0.79	0.2
$V_{2.75}Co_{0.25}Si$	2.95	0.81	0.24

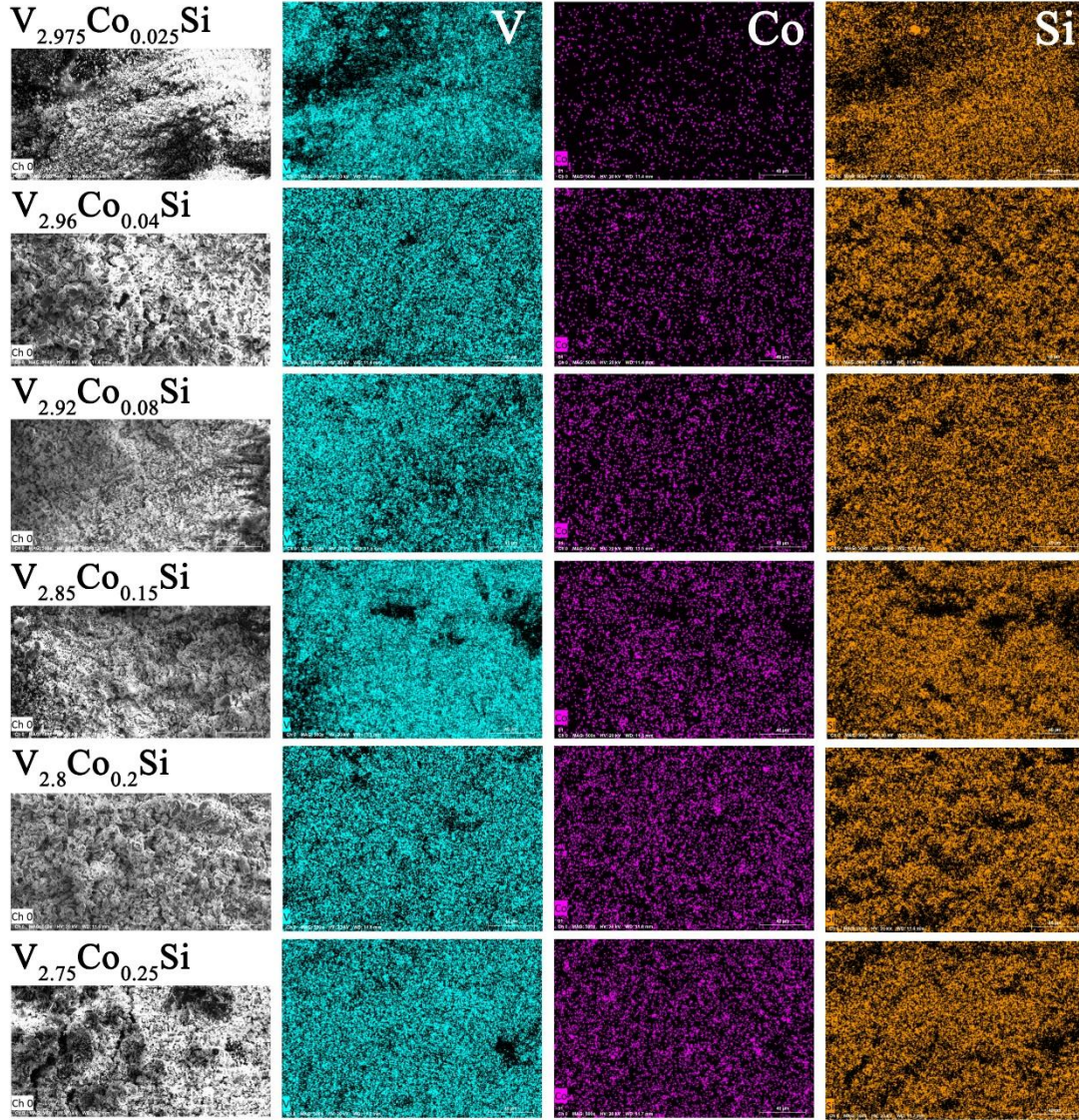


Fig. 2 SEM images and the corresponding EDS element mappings of $V_{3-x}Co_xSi$ ($0.025 \leq x \leq 0.25$).

The normalized resistivity of the $V_{3-x}Co_xSi$ ($0 \leq x \leq 0.30$) samples is shown in **Fig. 3**. The resistivity data for the $V_{3-x}Co_xSi$ system display the metallic behavior. The sharp drops can be observed in $\rho(T)$ for the $V_{3-x}Co_xSi$ ($0 \leq x \leq 0.30$) below 18 K, which signifies the onset of the superconducting state. The resistivity trend at a temperature between 8 -18 K is shown in **Fig. 3(a)**. The T_c was taken as the midpoint of the resistivity transitions. The T_c of the pristine V_3Si is 16.09 K, which is consistent with the previously reported value [29]. As the cobalt-doped content increases, the T_c decreases, and the superconducting transition width (ΔT_c) increases (see **Fig. 3(b)**). The

T_c is reduced from 16.09 K for the pristine sample to 10.5 K for $V_{2.7}Co_{0.3}Si$, while the ΔT_c is increased from 0.66 K to 3.40 K. Furthermore, a small amount of cobalt-doped content causes the residual resistivity ratio ($RRR = \rho_{300K}/\rho_{18K}$) value of the $V_{3-x}Co_xSi$ system to decrease rapidly and accompanied by the slight decrease in RRR value for higher cobalt-doped concentration.

Fig. 3(c) shows the temperature-dependent zero-field cooling (ZFC) dc magnetic susceptibility for the $V_{3-x}Co_xSi$ ($0 \leq x \leq 0.30$) samples. Measurements were performed between 2 K and 18 K under a 20 Oe applied magnetic field. It can be seen that strong superconducting diamagnetic signals appear in all samples. The critical temperature of T_c was determined as the value at the point where the linearly approximated slope crosses the zero value of normal state magnetization. To see the exact influence of the cobalt-doped content on T_c obtained from the susceptibility and resistivity measurements are shown in Table 1. The T_c values from magnetic and transport measurements are consistent. The T_c is roughly linearly decreased with increased cobalt-doped content.

Furthermore, when $x \geq 0.15$, the change in a knee can be observed on the diamagnetic curves, and the slope at the inflection point changes significantly. **Fig. 3(d)** displays the temperature derivative of susceptibility ($d\chi/dT$) for the $V_{3-x}Co_xSi$ ($0 \leq x \leq 0.30$) samples. The red arrows indicate the T_c s. We can observe small humps in the temperature range of 10 - 14 K, implying the superconductivity transition. In the low temperature, sharp peaks can be observed in $V_{3-x}Co_xSi$ ($0.15 \leq x \leq 0.30$) samples, corresponding to the knee on the diamagnetic curves. We define the lowest point between the two peaks (see inset in **Fig. 3(d)**), where the slope is the smallest, and the corresponding temperature is defined as T^* . It can be seen that the T^* decreases with increasing cobalt content. There may be a second superconducting phase or a structural phase transition at T^* .

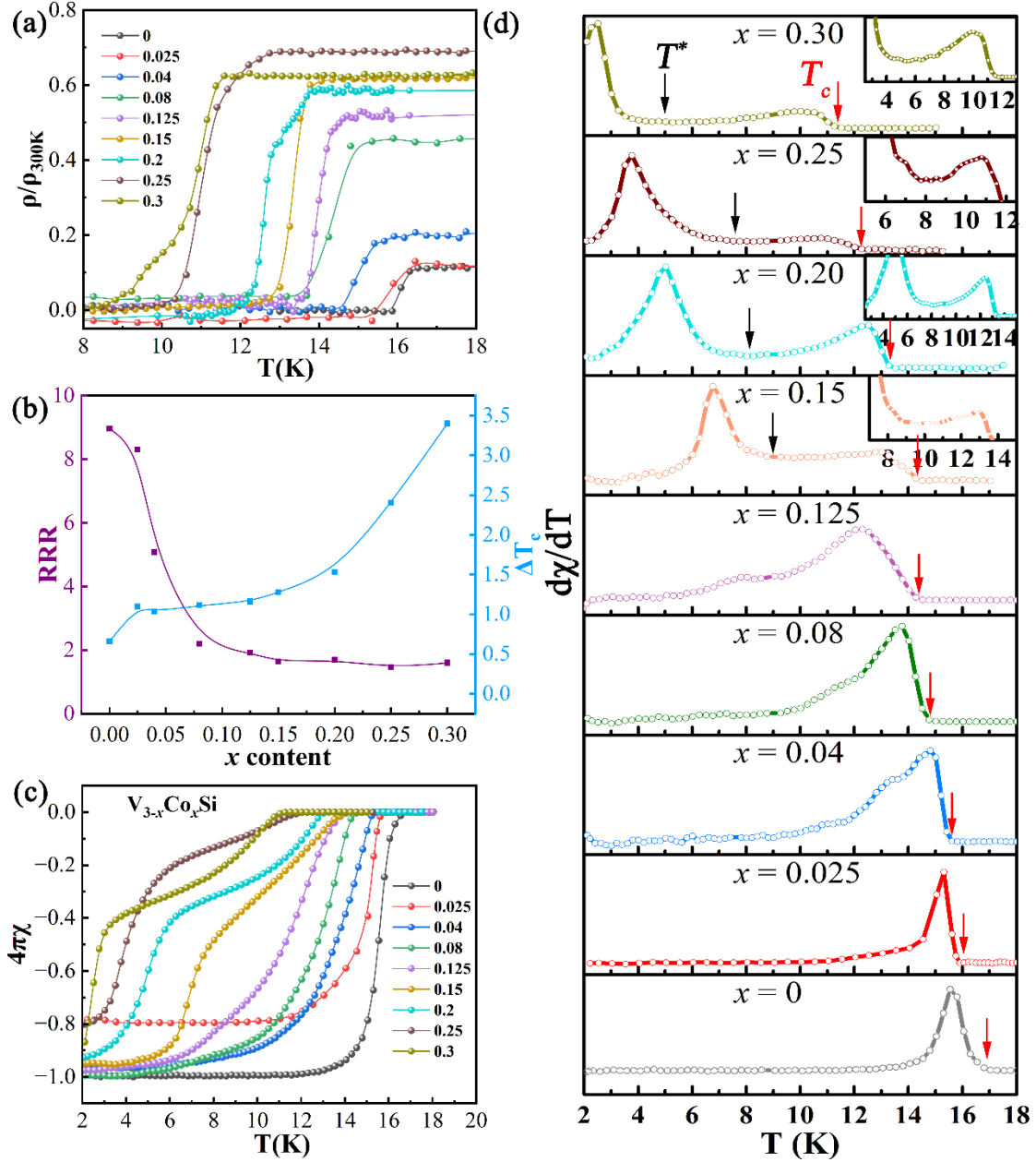


Fig. 3 (a) Normalized temperature-dependent resistivity of $V_{3-x}Co_xSi$ ($0 \leq x \leq 0.30$) alloys at the temperature range of 8-18 K. (b) cobalt content dependent on the RRR and ΔT_c values. (c) Magnetic characterization of $V_{3-x}Co_xSi$ ($0 \leq x \leq 0.30$) alloys with ZFC model. (d) the temperature derivative of susceptibility ($d\chi/dT$) for the $V_{3-x}Co_xSi$ ($0 \leq x \leq 0.30$) samples.

To further identify the lower critical field ($\mu_0 H_{c1}(0)$) of $V_{3-x}Co_xSi$ ($0 \leq x \leq 0.30$) alloys, the magnetization $M(H)$ curves at different temperatures are carried out, as shown in **Fig. 4**. The sample used for the susceptibility measurement is approximately cuboid in shape. And the magnetic field is applied in the direction of the cuboid c -axis.

The demagnetization factor (N) value is calculated from the equation $N = 4\pi\chi_v + 1$, where $\chi_v = dM/dH$ represents the slope of the linear fit. And the theoretical N value was calculated by the equation $N^{-1} = 1 + \frac{3}{4} \frac{c}{a} (1 + \frac{a}{b})$ [35], where $2a \times 2b \times 2c$ is the geometric parameters of cuboid. The geometric parameters of the susceptibility test sample are summarized in **Table 2**. At low magnetic fields, the data points have been fitted with the formula $M_{\text{fit}} = m + nH$, where m represents the intercept and n is the slope of the linear fitting. The M- M_{fit} dependence of the magnetic field is present in the insets of **Fig. 4**. The $\mu_0H_{c1}(0)$ can be obtained according to the formula $\mu_0H_{c1}^*(T) = \mu_0H_{c1}^*(0)(1-(T/T_c)^2)$. Due to demagnetization, the estimated value $\mu_0H_{c1}(0)$ should be modified using the formula $\mu_0H_{c1}(0) = \mu_0H_{c1}^*(0)/(1-N)$, where the demagnetization factor N of $V_{2.975}Co_{0.025}Si$ and V_3Si is 0.31 and 0.43, respectively. The N value has been used to correct the magnetic susceptibility data. The modified lower critical field $\mu_0H_{c1}(0)$ of $V_{2.975}Co_{0.025}Si$ and V_3Si is 120.0 mT and 138.0 mT, respectively. All the superconducting parameters are summarized in **Table 3**. It can be seen that with the increase of cobalt content, the $\mu_0H_{c1}(0)$ also gradually decreases.

Table 2. The geometric parameters of the susceptibility test sample.

Samples	Geometric parameters			Theoretical N value	Actual N value
	2b (mm)	2a (mm)	2c (mm)		
$x = 0$	2.55	1.21	0.98	0.53	0.43
$x = 0.025$	1.58	1.25	1.20	0.44	0.31
$x = 0.04$	2.01	1.36	0.99	0.52	0.31
$x = 0.08$	1.75	1.49	0.70	0.61	0.51
$x = 0.125$	1.35	0.99	1.20	0.39	0.36
$x = 0.15$	2.01	1.60	1.49	0.44	0.51
$x = 0.2$	1.38	1.03	1.16	0.40	0.40
$x = 0.25$	2.18	1.61	0.53	0.70	0.58
$x = 0.3$	1.98	1.65	1.24	0.49	0.51

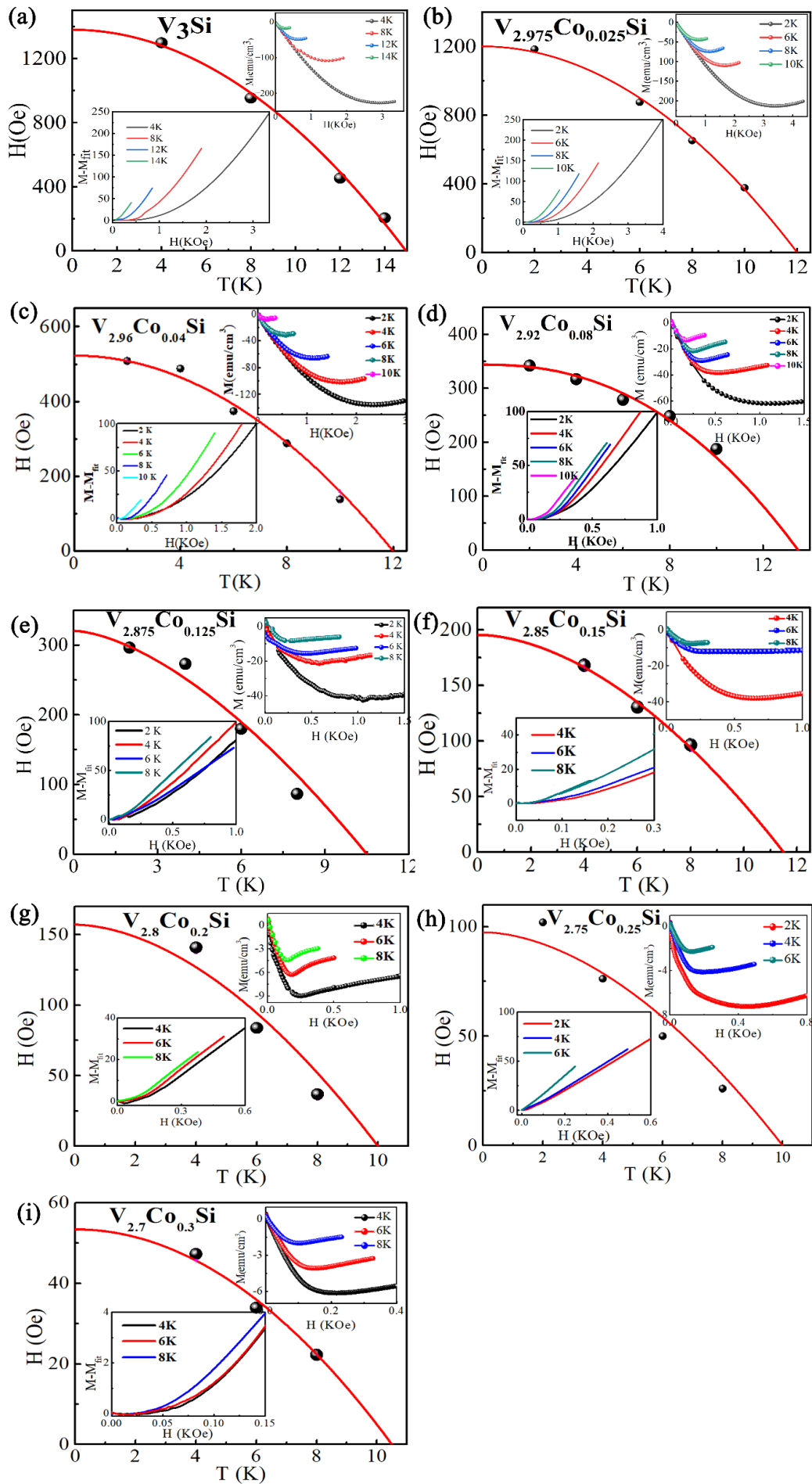


Fig. 4 The lower critical fields of $V_{3-x}Co_xSi$ ($0 \leq x \leq 0.30$) samples. The top right inset shows the $M(H)$ curves at different temperatures. The bottom left corner inset shows the $M-M_{fit}$ as a function of the applied field.

To reveal the upper critical magnetic field ($\mu_0H_{c2}(0)$), we conducted systematic measurements around the T_c under several magnetic fields of $V_{3-x}Co_xSi$ ($0 \leq x \leq 0.30$) alloys. As shown in **Fig. 5**, one can be seen that the shifting T_c towards lower temperatures is visible with applying higher magnetic fields. The $\mu_0H_{c2}(0)$ is obtained by fitting the 50 % criterion of normal state resistivity values using Werthamer-Helfand-Hohenberg (WHH) and Ginzburg-Landau (GL) models. The slope ($d\mu_0H_{c2}/dT$) of V_3Si , $V_{2.975}Co_{0.025}Si$, and $V_{2.96}Co_{0.04}Si$ can be obtained -2.163 T/K, -2.162 T/K, and -2.161 T/K, respectively, from the linear fitting. The $\mu_0H_{c2}(0)$ can then be estimated via the WHH equation: $\mu_0H_{c2}(0) = -0.693T_c(\frac{d\mu_0H_{c2}}{dT})|_{T=T_c}$. The calculated $\mu_0H_{c2}(0)$ of the WHH model for V_3Si , $V_{2.975}Co_{0.025}Si$, and $V_{2.96}Co_{0.04}Si$ are 34.89 T, 34.29 T, and 32.90 T, respectively. Additionally, we fit the Pauli limiting field (μ_0H^P) of $V_{3-x}Co_xSi$ ($0 \leq x \leq 0.30$) alloys by the formula $\mu_0H^P = 1.85 * T_c$, the values are present in **Table 3**. The experimentally estimated $\mu_0H_{c2}(0)$ values for all samples are very close to the Pauli limiting field. Furthermore, we can also obtain the $\mu_0H_{c2}(0)$ value of 30.57 T, 30.03 T, and 28.92 T for $V_{3-x}Co_xSi$ ($x = 0, 0.025, 0.04$) alloys fitted with GL formula: $\mu_0H_{c2}(T) = \mu_0H_{c2}(0) * \frac{1-(T/T_c)^2}{1+(T/T_c)^2}$. As displayed in **Fig. 5**, the distribution of spots obeys the function nicely. For comparison, we also calculated the $\mu_0H_{c2}(0)$ value of $V_{3-x}Co_xSi$ ($0.08 \leq x \leq 0.30$) samples. There are two superconducting transitions in the $V_{2.7}Co_{0.3}Si$ sample, possibly due to inhomogeneity. It can be seen that with the increase of cobalt content, the $\mu_0H_{c2}(0)$ also gradually decreases, except for the $V_{2.7}Co_{0.3}Si$ alloy.

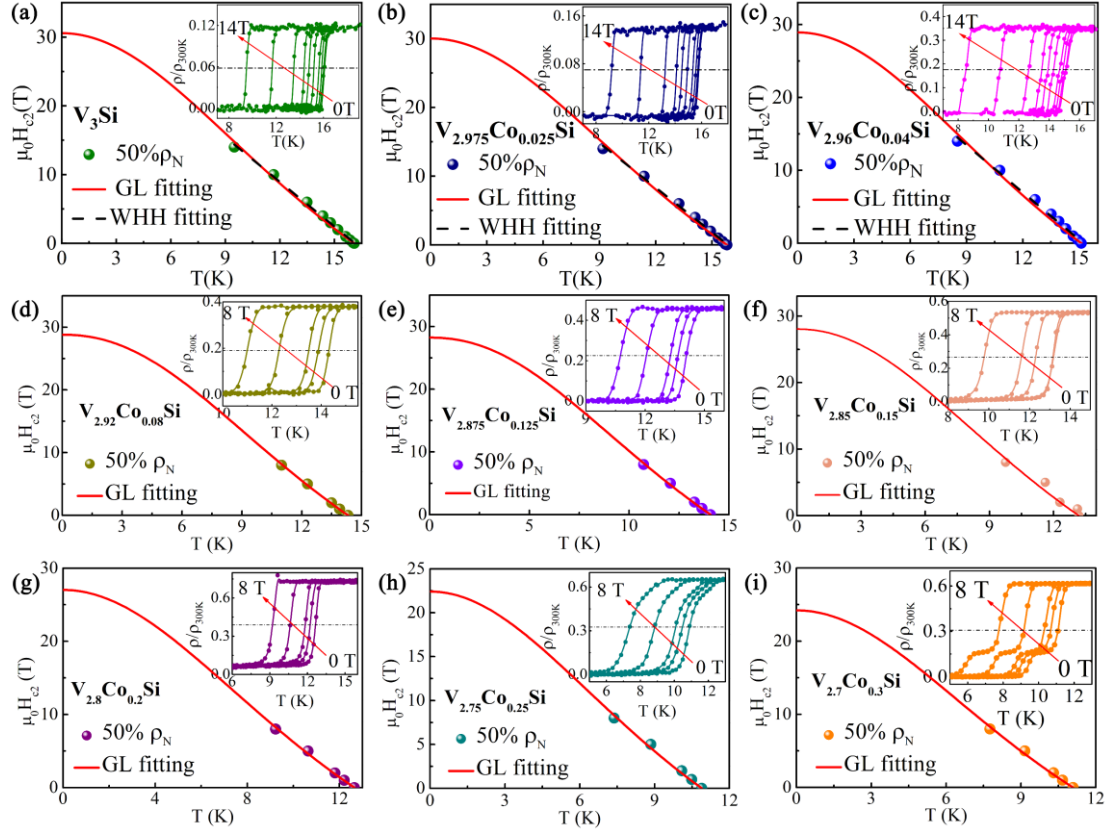


Fig. 5 The upper critical fields of $V_{3-x}Co_xSi$ ($0 \leq x \leq 0.30$) samples. The top right inset shows the low-temperature resistivity at different applied fields.

Table 3. Superconducting parameters of $V_{3-x}Co_xSi$ ($0 \leq x \leq 0.3$) alloys.

Cobalt content (x)	T_c^ρ (K)	T_c^χ (K)	RRR ($R_{300\text{K}}/R_{18\text{K}}$)	ΔT_c (K)	$\mu_0H_{c1}(0)$ (mT)	$\mu_0H_{c2}(0)$ (T)	μ_0H^P (T)
0	16.21	16.88	8.97	0.66	138.0	30.57	31.23
0.025	15.80	15.95	8.30	1.10	120.0	30.03	29.51
0.040	15.00	15.52	5.08	1.04	52.3	28.92	28.71
0.080	14.34	14.86	2.19	1.12	34.4	28.80	27.49
0.125	13.94	14.52	1.92	1.16	32.0	28.23	26.86
0.150	13.35	14.35	1.63	1.28	19.6	28.05	26.55
0.200	12.72	13.31	1.69	1.53	15.7	27.02	24.62
0.250	11.06	12.13	1.45	2.40	9.7	22.42	22.44
0.300	10.80	11.41	1.60	3.40	5.3	24.21	21.11

The specific heat measurement further characterizes the $V_{2.975}Co_{0.025}Si$ compound, as displayed in **Fig. 6(a)**. A sharp, specific heat jump can be observed, indicating the bulk nature of superconductivity. Meanwhile, the normal-state specific heat data have been fitted with the formula: $C_p/T = \gamma + \beta T^2$, where γ and β are the electronic and phonon-specific heat coefficients, respectively. The best fits give $\gamma = 0.15$ mJ/mol/K² and $\beta = 2.45 \times 10^{-4}$ mJ/mol/k⁴. After subtracting the phonon contribution, the electronic specific heat is isolated and plotted as C_{el}/T against temperature in **Fig. 6(b)**. Taking the entropy balance around the transition into account, a $T_c = 15.3$ K is obtained from the electronic-specific heat data, which agrees with the resistivity and magnetic susceptibility measurements (see **Table 3**). The electronic specific heat jump at T_c , $\Delta C_{el}/\gamma T_c = 1.99$, is larger than the value of 1.43 expected for the BCS weak coupling limit. Additionally, $C_{el}/T(T)$ decreases exponentially below T_c , suggesting an isotropic superconducting gap. The fitting performed quantitative analysis for electronic-specific heat data with a modified BCS model, the so-called α model, $C_{el}(T) = A \exp(-\Delta_0/k_B T)$, where Δ_0 and k_B are the superconducting gap at 0 K and Boltzmann constant, respectively. Here the coupling constant α is defined as $\alpha \equiv \Delta_0/T_c$, and the BCS weak-coupling limit $\alpha = 1.76$ (the black dash line in **Fig. 6(b)**). The obtained $\alpha = 1.20$ (solid blue line in **Fig. 5(b)**) gives an excellent fit. Furthermore, the Debye temperature (Θ_D) can be calculated with the following formula: $\Theta_D = (12\pi^4 nR/5\beta)^{1/3}$, where $n = 4$ represents the number of atoms per unit cell. It yields $\Theta_D = 3161$ K for $V_{2.975}Co_{0.025}Si$. Once Θ_D is calculated, the electron-phonon coupling strength λ_{ep} can be obtained via the inverted McMillan equation: $\lambda_{ep} = \frac{1.04 + \mu^* \ln\left(\frac{\Theta_D}{1.45T_c}\right)}{(1 - 0.62\mu^*) \ln\left(\frac{\Theta_D}{1.45T_c}\right) - 1.04}$, where the Coulomb pseudopotential parameter $\mu^* = 0.13$ [26,27]. It yields $\lambda_{ep} = 0.48$ for $V_{2.975}Co_{0.025}Si$ compound.

As a comparison, we also performed the heat capacity measurement on the sample with high cobalt content. **Fig. 6(c)** displays the $C_p/T(T)$ curves of $V_{2.8}Co_{0.2}Si$ down to 2 K at 0 T and 5 T fields. However, two specific heat jumps can be observed in **Fig.**

6(c), one of which has a minor anomaly in heat capacity data. The clear anomaly jump is around 12.3 K at 0 T field, which is consistent with the T_c in Table 1. Meanwhile, the normal-state specific heat data also fitted with the following formula: $C_p/T = \gamma + \beta T^2$, giving $\gamma = 17.61$ mJ/mol/K² and $\beta = 0.06$ mJ/mol/k⁴. **Fig. 6(b)** shows the $C_{el}/T(T)$ curves at a temperature between 2 - 20 K under 0 T. Using the standard equal-area entropy construction method, and we can determine $\Delta C_{el}/\gamma T_c = 1.22$, which is slightly smaller than the BCS weak coupling limit (1.43), revealing its superconducting nature. Based on the above parameters, the Θ_D and λ_{ep} are calculated to be 506 K and 0.72, respectively. The inset in **Fig. 6(c)** displays the $C_p/T(T^2)$ data at low temperatures. Comparing the heat capacity data under the applied magnetic field of 0 T and 5 T, the external magnetic field will suppress the T_c , corresponding to the specific heat peak of the superconducting transition moving to a lower temperature. However, the minor anomaly in $C_p/T(T^2)$ curves around 8.5 K did not change under an external magnetic field of 5 T, which can rule out superconductivity and magnetic transitions. Interestingly, this minor anomaly of 8.5 K in the $V_{2.8}Co_{0.2}Si$ heat capacity coincides with the T^* in $d\chi/dT$ curves. We speculated that a structural phase transition may have occurred at T^* in the high-content cobalt-doping samples ($x \geq 0.15$). Previous studies have shown a martensitic cubic to tetragonal phase transition at the temperature of about 18.9 K in the V_3Si compound [16-19]. Besides, the hydrostatic pressure will gradually suppress this martensitic phase transition [36,37]. Cobalt-doping reduces the lattice parameters, which may be equivalent to applying external pressure. And the T^* decreases with increasing cobalt content (see Fig. 2(d)). The $V_{2.8}Co_{0.2}Si$ sample may have undergone a martensitic transformation at about 8.5 K. Furthermore, an in-depth study is warranted to understand the present experimental findings.

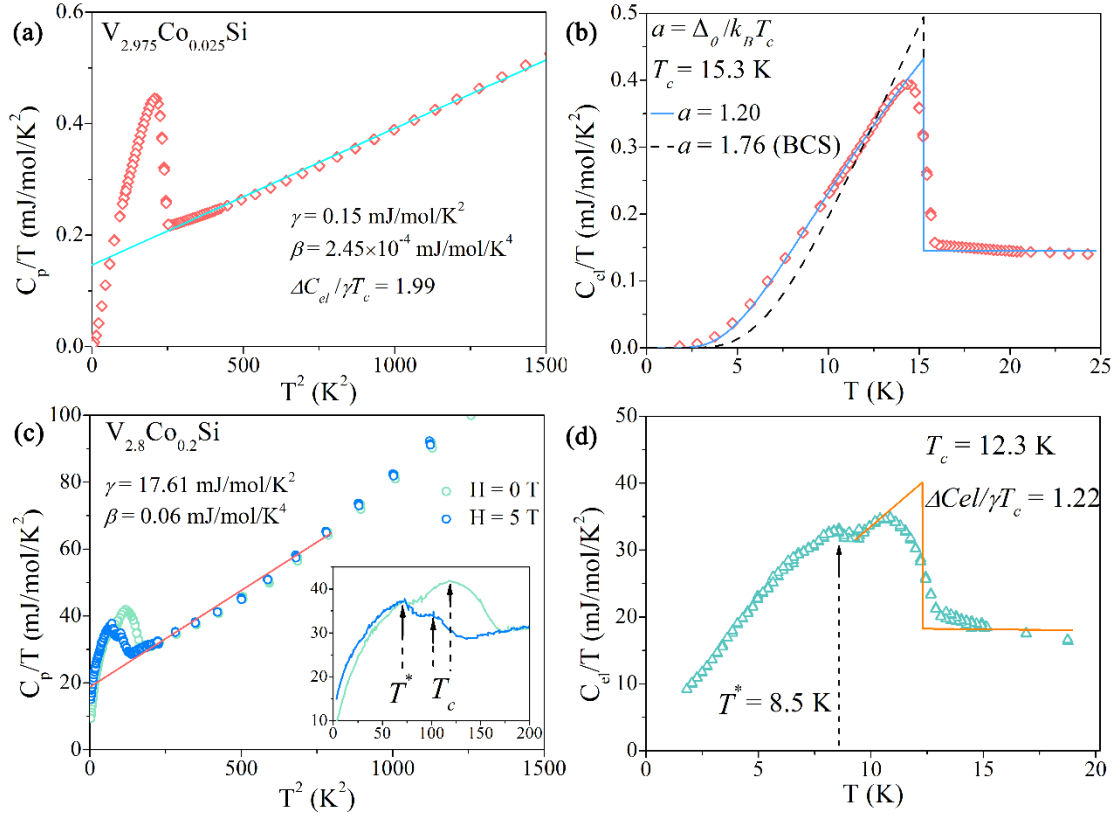


Fig. 6 (a) $C_p/T(T^2)$ curves of $V_{2.975}Co_{0.025}Si$ alloy without magnetic field. (b) Temperature dependence of the electronic specific heat C_{el} of $V_{2.975}Co_{0.025}Si$ alloy. (c) $C_p/T(T^2)$ curves of $V_{2.8}Co_{0.2}Si$ alloy at 0 T and 5 T field. The inset shows the $C_p/T(T^2)$ curves at low temperatures. (d) Temperature dependence of the electronic specific heat C_{el} of $V_{2.8}Co_{0.2}Si$ alloy.

Fig. 7 plots the T_c of $V_3Si_{1-x}Ga_x$ [30], $V_3Si_{1-x}Al_x$ [30], and $V_{3-x}Co_xSi$ A15 structure superconductors as a function of the electron/atom (e/a) ratio. Whether doping gallium/aluminum on silicon or cobalt on vanadium will decrease the T_c of V_3Si , when considering the e/a ratio in the V_3Si system, it can be found that the substitution of gallium/aluminum for silicon reduces the e/a ratio and the substitution of cobalt for vanadium increases the e/a ratio. We also illustrate the trend lines of the T_c of transition metals and their alloys in crystalline form and as amorphous vapor-deposited films for comparison [38]. It is often referred to as the Matthias rule, which shows the T_c maximum occurs at around 4.7 e/a for transition metals, even though the maximum is much broader than simple crystalline superconductors. As the e/a ratio increases, the T_c variation trend of V_3Si is as pronounced as in crystalline alloys and monotonically

follows the trend observed for amorphous superconductors. The V_3Si has the maximum T_c with electron count $e/a = 4.7$, which is the essential feature of the Matthias rule, indicating that chemical doping makes it challenging to increase the T_c of V_3Si bulk. Furthermore, according to the rigid band model and the electronic structure calculations of V_3Si [39], cobalt doping at the vanadium site will increase the number of VECs in the unit cell, resulting in the increase of the Fermi energy E_F and the decrease of $N(E_F)$.

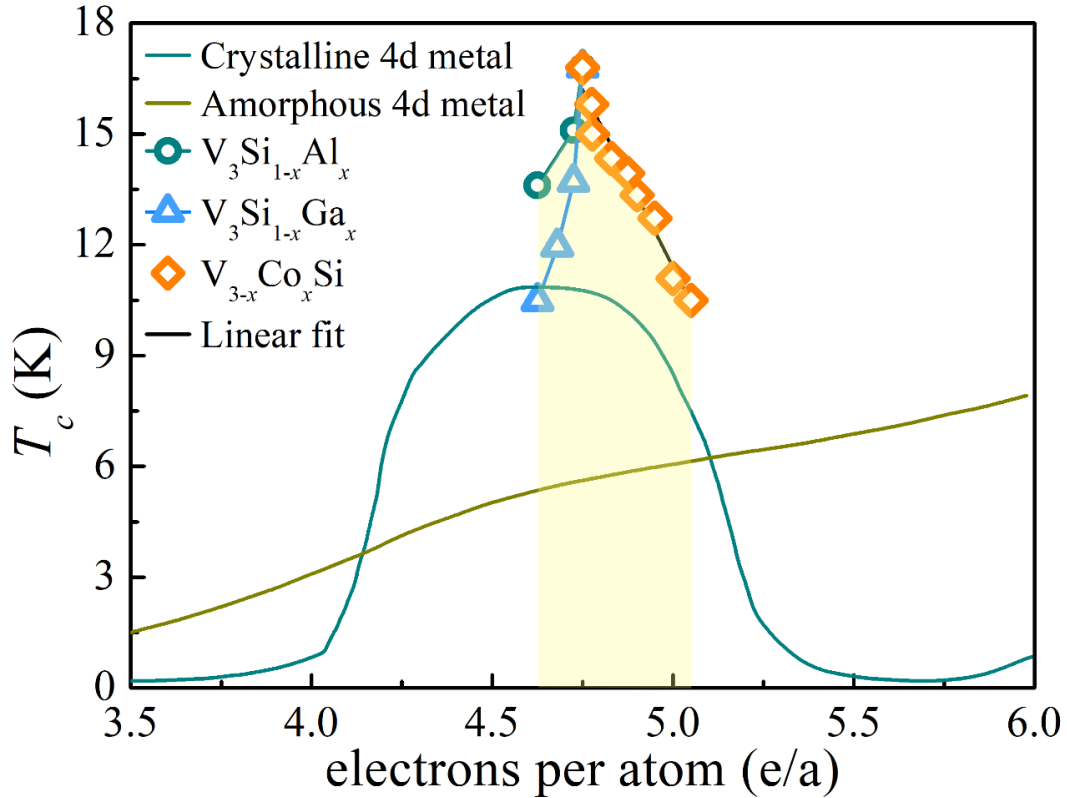


Fig. 7 valence electron count per atom dependency of the T_c of $V_3Si_{1-x}Al_x$ [30], $V_3Si_{1-x}Ga_x$ [30], and $V_{3-x}Co_xSi$ systems.

Conclusion

We have synthesized $V_{3-x}Co_xSi$ alloys with x up to 0.3 by an arc melting method and subsequent annealing. According to PXRD refinement data, the increase of cobalt-doped content decreases the lattice parameter. Resistivity and susceptibility measurements show an almost linear decrease in T_c with increasing cobalt content in the $V_{3-x}Co_xSi$ system. The V_3Si has the maximum T_c with electron count $e/a = 4.7$, which is an essential feature of the Matthias rule. The relationship between T_c and e/a

ratio in the $V_{3-x}Co_xSi$ system is almost linear. The RRR values indicate that cobalt doping introduces disorder in the $V_{3-x}Co_xSi$ system, and the following leads to a suppression of the critical temperature T_c . Further, with higher Co-doped content, $V_{3-x}Co_xSi$ ($0.15 \leq x \leq 0.30$) alloys may have superconducting and structural phase transitions. The fitted data show that cobalt doping also reduces the critical field of the $V_{3-x}Co_xSi$ system. Type-II superconductivity is demonstrated on all $V_{3-x}Co_xSi$ samples.

Acknowledgments

This work is supported by the National Natural Science Foundation of China (11922415, 12274471, 22205091), Guangdong Basic and Applied Basic Research Foundation (2022A1515011168, 2019A1515011718, 2019A1515011337), the fund of State Key Laboratory of Optoelectronic Materials and Technologies (OEMT-2022-ZRC-02), the Key Research & Development Program of Guangdong Province, China (2019B110209003), and the Pearl River Scholarship Program of Guangdong Province Universities and Colleges (20191001).

References

- [1] H Hosono, A Yamamoto, H Hiramatsu and Y W Ma 2018 *Mater. Today* 21 278-302
- [2] G R Stewart 2015 *Physica. C* 514 28-35
- [3] L R Testardi 1971 *Phys. Rev. B* 3 95-106
- [4] R Viswanathan and H Luo 1971 *Solid State Commun. (USA)* 9 1733-36
- [5] M Dayan, A M Goldman, C C Huang, M C Chiang and L E Toth 1979 *Phys. Rev. Lett.* 42 335-38
- [6] J R Gavaler, M A Janocko and C K Jones 1974 *J. Appl. Phys. (USA)* 45 3009-13
- [7] L R Testardi, J H Wernick and W A Royer 1974 *Solid State Commun. (USA)* 15 1-4
- [8] M Kim, C Z Wang and K M Ho 2019 *Phys. Rev. B* 99 235423
- [9] J Muller 1980 *Rep. Prog. Phys. (UK)* 43 641-87
- [10] J W Blezjus and J P Carbotte 1986 *Phys. Rev. B* 33 3509-11
- [11] M N Khlopkin 1999 *JETP. Lett+* 69 26-30
- [12] V G Kogan, C Martin and R Prozorov 2009 *Phys. Rev. B* 80 014507
- [13] L R Testardi, J M Poate and H J Levinstein 1977 *Phys. Rev. B, Solid State (USA)* 15 2570-80

- [14] F M Mueller, D H Lowndes, Y K Chang, A J Arko, and R S List 1992 *Phys. Rev. Lett* 68 3928-31
- [15] W D Wu, A Keren, L P Le, G M Luke, B J Sternlieb, Y J Uemura, D C Johnston, B K Cho and P Gehring 1994 *Hyperfine Interact. (Switzerland)* 86 615-21
- [16] R Mailfert, B W Batterman and J J Hanak 1967 *Phys. Lett. A* 24 315-16
- [17] A Sauer, D A Zocco, A H Said, R Heid, A Bohmer and F Weber 2019 *Phys. Rev. B* 99 134511
- [18] H M Tütüncü, H Y Uzunok, G P Srivastava, V Özdemir and G Uğur 2018 *Intermetallics* 96 25-32
- [19] R Viswanathan and D C Johnston 1976 *Phys. Rev. B* 13 2877-79
- [20] G Shirane, J D Axe and R J Birgeneau 1971 *Solid State Commun. (USA)* 9 397-400
- [21] M Yethiraj 2002 *Appl. Phys. A-Mater* 74 S1210-S12
- [22] K Cho, M Konczykowski, S Ghimire, M A Tanatar, L L Wang, V G Kogan and R Prozorov 2022 *Phys. Rev. B* 105 024506
- [23] J Nagamatsu, N Nakagawa, T Muranaka, Y Zenitani and J Akimitsu 2001 *Nature* 410 63-64
- [24] T D Vethaak, F Gustavo, T Farjot, T Kubart, P Gergaud, S L Zhang, F Lefloch and F Nemouchi 2021 *Microelectron. Eng.* 244-246 111570
- [25] W Zhang, A T Bollinger, R Li, K Kisslinger, X Tong, M Liu and C T Black 2021 *Sci. Rep.* 11 2358
- [26] L Y Zeng, X W Hu, N N Wang, J P Sun, P T Yang, M Boubeche, S J Luo, Y Y He, J G Cheng, D X Yao and H X Luo 2022 *J. Phys. Chem. Lett.* 13 2442-51
- [27] L Y Zeng, Y Ji, D P Yu, S Guo, Y Y He, K Li, Y H Huang, C Zhang, P F Yu, S J Luo, H C Wang and H X Luo 2022 *J. Phys. Chem. C* 126 3705-12
- [28] B A Hatt, J K R Page and V G Rivlin 1973 *J. Low Temp. Phys.* 10 285-98
- [29] B He, C Dong, L M Zeng, H R Liu, L H Yang and H Chen 2008 *Supercond. Sci. Tech.* 21 035004
- [30] G Otto 1969 *Zeitschrift für Physik* 218 52-55
- [31] C Wang, Y K Li, Z W Zhu, S Jiang, X Lin, Y K Luo, S Chi, L J Li, Z Ren, M He, H Chen, Y T Wang, Q Tao, G H Cao and Z A Xu 2009 *Phys. Rev. B* 79 051521
- [32] P Yuan, J Han, P Cheng, R Ma, Q Xiao, J Ge, Z Feng, S Cao, J Zhang, W Lu and F Chen 2021 *J. Phys.: Condens. Mater* 33 335601
- [33] S Elizabeth, A Anand, S V Bhat, S V Subramanyam and H L Bhat 1999 *Solid State Commun* 109 333-38
- [34] J Prakash, S J Singh, S Patnaik and A K Ganguli 2009 *Solid State Commun* 149 181-83
- [35] R Prozorov and V G Kogan 2018 *Phys. Rev. Applied* 10 014030
- [36] C W Chu and L R Testardi 1974 *Phys. Rev. Lett.* 32 766-69
- [37] L R Testardi 1975 *Rev. Mod. Phys.* 47 637-48
- [38] M M Collver and R H Hammond 1979 *Phys. Rev. B, Condens. Matter (USA)* 19 525-26

[39] B M Klein, L L Boyer, D A Papaconstantopoulos and L F Mattheiss 1978
Phys. Rev. B 18 6411-38